

Passive InP regenerator integrated on SOI for the support of broadband silicon modulators

M. Tassaert,^{1,*} H. J. S. Dorren,² G. Roelkens,¹ and O. Raz²

¹Photonics Research Group - Ghent University/imec,
Sint-Pietersnieuwstraat 41, 9000 Gent, Belgium

²Eindhoven University of Technology, Den Dolech 2, 5600MB, Eindhoven, The Netherlands

*martijn.tassaert@intec.ugent.be

Abstract: Passive signal regeneration based on the Membrane InP Switch (MIPS) is demonstrated. Because of the high confinement of light in the active region of the MIPS, the device acts as a saturable absorber with a highly non-linear response. Using this effect, the extinction ratio (ER) of low-ER signals can be tripled and a receiver sensitivity enhancement of 4.5 dB is demonstrated using an input signal at 1 Gb/s with an ER of 2 dB. Regenerator operation up to 5 Gb/s is demonstrated and using a device simulator a strategy to reach higher bitrate operation is proposed.

© 2012 Optical Society of America

OCIS codes: (130.3120) Integrated optics devices; (200.6015) Signal regeneration.

References and links

1. A. Barkai, Y. Chetrit, O. Cohen, R. Cohen, N. Elek, E. Ginsburg, S. Litski, A. Michaeli, O. Raday, D. Rubin, G. Sarid, N. Izhaky, M. Morse, O. Dosunmu, A. Liu, L. Liao, H. Rong, Y. Kuo, S. Xu, D. Alduino, J. Tseng, H.-F. Liu, and M. Paniccia, "Integrated silicon photonics for optical networks [Invited]," *J. Opt. Netw.* **6**, 25–47 (2007).
2. Y. Vlasov, "Silicon photonics for next generation computing systems [Tutorial]," presented at the 34th European Conference on Optical Communication (ECOC 2008), Brussels, Belgium, 21–25 Sept. 2008.
3. D. Van Thourhout, T. Spuesens, S. Selvaraja, L. Liu, G. Roelkens, R. Kumar, G. Morthier, P. Rojo-Romeo, F. Mandorlo, O. Raz, C. Kopp, and L. Grenouillet, "Nanophotonic devices for optical interconnect," *IEEE J. Sel. Top. Quantum Electron.* **16**, 1363–1375 (2010).
4. G. Roelkens, L. Liu, D. Liang, R. Jones, A. Fang, B. Koch, and J. Bowers, "III-V/silicon photonics for on-chip and inter-chip optical interconnects," *Laser Photon. Rev.* **4**, 751–779 (2010).
5. G. Reed, G. Mashanovich, F. Gardes, and D. Thomson, "Silicon optical modulators," *Nat. Photonics* **4**, 518–526 (2010).
6. W. Bogaerts, L. Liu, S. Selvaraja, J. Brouckaert, D. Taillaert, D. Vermeulen, G. Roelkens, D. Van Thourhout, and R. Baets, "Silicon nanophotonic waveguides and their applications," *Proc. SPIE* **7134**, 71341O-1 (2008).
7. L. Liao, D. Samara-Rubio, M. Morse, A. Liu, D. Hodge, D. Rubin, U. D. Keil, and T. Franck, "High speed silicon Mach-Zehnder modulator," *Opt. Express* **13**, 3129–3135 (2005).
8. N. Feng, S. Liao, D. Feng, P. Dong, D. Zheng, H. Liang, R. Shafiqi, G. Li, J. Cunningham, A. Krishnamoorthy, and M. Asghari, "High speed carrier-depletion modulators with 1.4V-cm $V_{\pi}L$ integrated on 0.25 μm silicon-on-insulator waveguides," *Opt. Express* **18**, 7994–7999 (2010).
9. D. Miller, "Device requirements for optical interconnects to silicon chips," *Proc. IEEE* **97**, 1166–1185 (2009).
10. M. Tassaert, G. Roelkens, H. Dorren, D. Van Thourhout, and O. Raz, "Bias-free, low power and optically driven membrane InP switch on SOI for remotely configurable photonic packet switches," *Opt. Express* **19**, B817–B824 (2011).
11. M. Tassaert, S. Keyvaninia, D. Van Thourhout, W. Green, Y. Vlasov, and G. Roelkens, "A nanophotonic InP/InGaAlAs optical amplifier integrated on a silicon-on-insulator waveguide circuit," in *Proceedings of IEEE Conference on Information Photonics 2011* (2011), Vol. 1–2.

1. Introduction

The current tendency in computing is directed towards parallelism on all levels. As systems consist of an increasing number of components working together, the amount of data that needs to be sent across a chip and in between different system components increases as well. Electronics are fundamentally limited in the achievable bandwidth–distance product and therefore an alternate solution needs to be found. With the advances in photonic integration technology, an integrated optical solution has become feasible. However, to be cost effective, the fabrication should be CMOS compatible. In this context, silicon photonics has seen increasing interest in industry [1, 2] and academia [3–5]. Although silicon is an excellent material to realize passive optical functions [6], the realization of active components is more challenging due to silicon's indirect band gap. Using heterogeneous integration of III-V on silicon, light sources and detectors have already been successfully demonstrated [4]. Another critical component for the realization of high performance on-chip optical interconnects is an optical modulator. Using the plasma dispersion effect, high-speed, low-power devices based on resonant cavities have been demonstrated in silicon [5]. However, due to their narrow bandwidth, device operation is vulnerable to temperature variations and fabrication errors. To allow broadband operation, solutions based on a Mach-Zehner interferometer (MZI) have been proposed. The drawback of these however, is that the $V_{\pi}L_{\pi}$ product is typically of the order of 1.0 Vcm [7, 8], implying that modulators either need to be long or require high voltages to achieve a high extinction ratio (ER). Furthermore the free carrier absorption effect causes considerable insertion losses. To make optical interconnects competitive with their electrical counterpart, the power consumption should be lower [9], which corresponds to a reduction of the operating voltage and device length of the modulator. This implies however that the achieved ER in the generated signal will be low, leading to a high receiver power penalty. Therefore, it would be beneficial to find a method with low power consumption for increasing the ER of a signal on a silicon circuit.

In this paper, we report on the use of the recently introduced membrane InP switch (MIPS) for on-chip regeneration of low-ER signals [10]. A 4.5 dB receiver sensitivity improvement for a 2 dB input ER signal is demonstrated at a modulation speed of 1 Gb/s and operation up to 5 Gb/s is shown. Furthermore, the good match between these measurements and simulated results give confidence that simulated 10 Gb/s operation can soon be experimentally demonstrated when a modified device layout is fabricated.

2. Device layout and operating principle

The device layout of the MIPS is schematically shown in Fig. 1(a). The MIPS consists of a heterogeneously integrated III-V membrane waveguide, which is coupled to two underlying silicon waveguides using two inverted taper couplers. In these couplers, the 220 nm thick silicon wire linearly tapers from a width of 700 nm down to a width of 100 nm, while the III-V membrane above tapers from 1 μ m to 2 μ m over a length of 18 μ m to ensure adiabatic coupling of the fundamental TE-mode. The III-V membrane waveguide is a 2 μ m broad rib waveguide of only 100 nm thick. It is made by shallow etching a bonded III-V epitaxial layer stack, which consists of three 8 nm thick InGaAs quantum wells (QWs), separated by 10 nm thick InP barriers layers. This QW stack is sandwiched between two 25 nm thick InP cladding layers. The QW band gap was determined to be at a wavelength of 1.58 μ m. A rib waveguide structure is used because the shallow etched cladding layers create a path along which dissipated heat can escape, significantly reducing the thermal resistance [11]. Because of the high index contrast between the III-V waveguide and the surrounding DVS-BCB/SiO₂ cladding layer, the confinement in the three QWs reaches a value of 17%. This can be clearly seen in Fig. 1(b), where the fundamental TE-mode of the III-V waveguide is shown. This high confinement makes the MIPS ideal to use as a saturable absorber. This is the case because the differential modal absorption $\partial\alpha/\partial N$

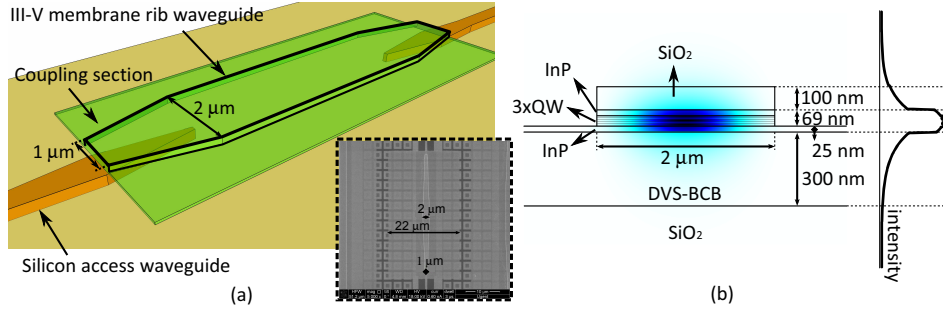


Fig. 1. (a) Schematic view of the device. In the inset, a SEM image of a $40\ \mu\text{m}$ long device is shown. (b) The mode profile in the III-V membrane waveguide and cross section of the intensity in the center of the waveguide.

is proportional to the confinement in the QWs. Therefore, the device absorption will rapidly change with changing carrier concentration. Moreover, these carriers are generated by the absorption of the signal beam itself, which is again proportional with the confinement. These two combined effects lead to a strong non-linearity in the transmission through the MIPS, which can be used for regeneration. The MIPS is coupled to input and output fibers by using a horizontal coupling scheme, in which light is first coupled from the silicon waveguides to a cleaved $1.5\ \mu\text{m}$ thick SU-8 waveguide, which has a width of $3\ \mu\text{m}$ to have a good modal overlap with a lensed fiber. A Scanning Electron Microscopy (SEM) image of a fabricated device can be seen in the inset of Fig. 1(a) and the details on the fabrication can be found in [10].

3. Device simulation

To gain more insight in the characterization results, a device simulator was created. The following free carrier equation was used:

$$\frac{\partial N(z,t)}{\partial t} = \frac{\tilde{P}_{abs}(z,t)}{h\nu A_{QW}} - \frac{N(z,t)}{\tau_c} - BN(z,t)^2 - CN(z,t)^3 \quad (1)$$

in which N is the free carrier concentration in the QWs, \tilde{P}_{abs} the absorbed power in the QWs per length unit, A_{QW} the total QW cross section area, τ_c the non-radiative carrier lifetime, B and C respectively the spontaneous and auger recombination coefficient for InGaAs at 300 K. To model the optical power in the device and derive \tilde{P}_{abs} , the following was used:

$$\frac{\partial P(z,t)}{\partial z} = (-\Gamma\alpha_{mat}(z,t) - \Gamma\alpha_{fca}(z,t) - \alpha_{scat})P(z) \quad (2)$$

$$\tilde{P}_{abs} = \frac{\Gamma\alpha_{mat}(z,t)}{\Gamma\alpha_{mat}(z,t) + \Gamma\alpha_{fca}(z,t) + \alpha_{scat}} \frac{\partial P}{\partial z} \quad (3)$$

Γ is the confinement in the QWs. α_{scat} was assumed to be fixed at a value of 4 dB/cm, the free carrier absorption α_{fca} is modeled as $k_{fca}N(z,t)$ and the material absorption is

$$\alpha_{mat}(z,t) = \alpha_0(\lambda) (1 - N(z,t)/N_t(\lambda)) \quad (4)$$

Here α_0 is the material absorption when no pumping power is applied and N_t is the transparency carrier density. α_0 was extracted from previous measurements on a comparable set of devices, by considering the device absorption of a low-power signal beam through different device lengths. The resulting absorption values were then fitted to a quadratic curve, which yields

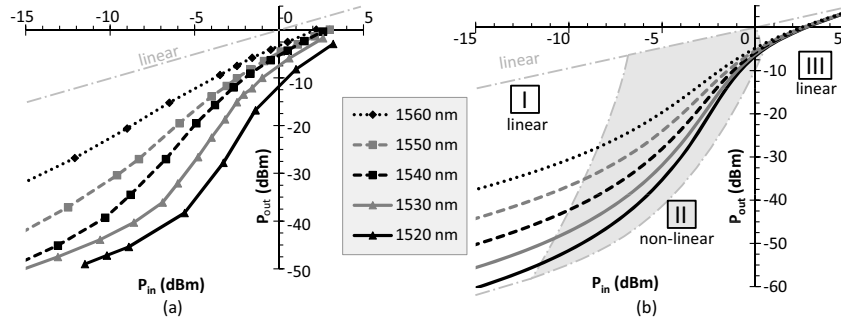


Fig. 2. (a) Transmission measurements through a $150\ \mu\text{m}$ long device. Input and output power are on-chip powers, which were derived by subtracting the measured fiber-to-chip coupling loss from the data (6.5 dB). (b) Simulated transmission through this device.

for 1530 nm, 1550 nm and 1570 nm respectively $-5800/\text{cm}$, $-4230/\text{cm}$ and $-2175/\text{cm}$. N_t was extracted by fitting earlier measured pump-probe measurement data, yielding $N_t = 1.6 \times 10^{18}/\text{cm}^3$ [10]. In this model, the longitudinal diffusion of carriers was neglected, as the length scale over which the absorption changes is much higher than the typical diffusion length. These equations were numerically integrated using the fifth order Adams–Bashforth method.

4. Characterization

4.1. Static non-linearity

To assess the potential regeneration performance of the MIPS, the static transmission curves have been measured for different wavelengths in a $150\ \mu\text{m}$ long device. The measurement results are shown in Fig. 2(a) and the corresponding simulation results are given in Fig. 2(b). The MIPS shows a large non-linear response. There are three regimes in the device operation. For low operating powers, the device absorption is barely bleached and therefore the output power varies linearly with the input power. When power increases however, the amount of generated carriers starts reducing the device absorption and a $\partial P_{out}/\partial P_{in}$ slope of more than one is achieved. In this region, the MIPS could act as a regenerator. For wavelengths further away from the band gap wavelength, the achieved slope is very steep, up to a value of 5 for wavelengths shorter than 1530 nm. For high signal powers, the device is completely bleached and the output power is almost equal to the input power. At shorter wavelengths, there is a discrepancy between the simulation results and the measurement results. This is probably caused by a varying fiber-to-chip coupling loss, while this was assumed constant at 6.5 dB in all measurements here. This coupling value was determined by measuring the transmission at a wavelength of $1.6\ \mu\text{m}$, for which there is no material absorption.

4.2. Regeneration experiment

In order to establish the regeneration operation of the MIPS, a bit error rate (BER) measurement was performed using the setup depicted in Fig. 3. In these experiments a pseudorandom binary sequence (PRBS) of $2^{31} - 1$ bits was used, imprinted on the CW light carrier using non return to zero on-off keying (NRZ-OOK).

In a first experiment the achieved ER and associated insertion loss were measured as a function of input power, for an input signal with an ER of 2 dB at a bitrate of 1 Gb/s. The results of this experiment are shown in Fig. 4(a). This graph displays clearly a trade-off between the efficiency of the regeneration action and the insertion loss. For a lower input power, the insertion loss is higher but the input power is closer to the optimal working point for regeneration,

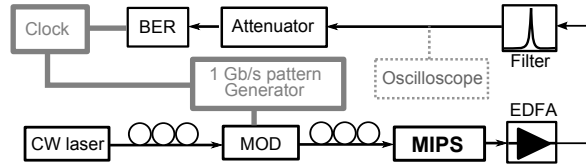


Fig. 3. Setup used for the regeneration experiment.

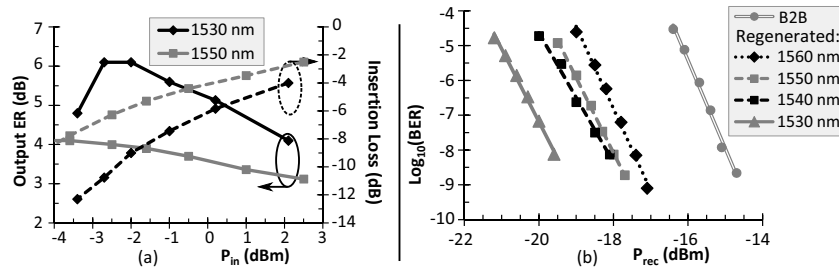


Fig. 4. (a) Achieved ER and associated insertion loss as a function of input power. (b) Measured BER as a function of average received power at 1 Gb/s.

resulting in a higher output ER. Furthermore, as was already stated in section 4.1, the achieved $\partial P_{out}/\partial P_{in}$ slope is steeper for wavelengths further away from the band gap, resulting in better regeneration. However, as the device is not completely bleached in the optimal region for regeneration and the device absorption is higher for shorter wavelengths, this comes at the cost of a higher insertion loss.

Using this data, the optimal input power for regeneration could be determined and a BER measurement at 1 Gb/s was performed. In this experiment a back-to-back (B2B) measurement was compared to a measurement on the regenerated signals for different wavelengths. The results are shown in Fig. 4(b). It is clear that the achieved ER improvement also leads to the expected reduction in power penalty. For a -1.5 dBm signal at 1530 nm, the improved ER from 2 dB to 6.2 dB leads to an expected 4.5 dB reduction in necessary received power to achieve error-free ($BER < 10^{-9}$) transmission. This can also be seen in the eye diagram in Fig. 5(a). For longer wavelengths, the achieved reduction is lower. Based on the non-linear transmission curves in Fig. 2 however, a receiver sensitivity improvement of over 3 dB over the entire C-band can be expected, if a QW stack with a modified band gap at $1.6 \mu\text{m}$ would be used.

5. Device speed

An operating bitrate of 1 Gb/s is rather low for practical application of such a device. From the eye diagram in Fig. 5(a), it can be seen that device operation is already near its speed limit at 1 Gb/s. Therefore, to achieve higher bitrates the device will need to be sped up. One way to achieve this, is by bleaching the MIPS faster. From the simulation, we can calculate the energy required to bleach the device, which is of the order of 0.6 pJ. By using a higher signal power, this energy can be delivered faster, resulting in a shorter signal rise time. To demonstrate this, a signal with 2 dB ER at 1530 nm was sent through the device at a bitrate of 5 Gb/s using 6 dBm on-chip power. In Fig. 5(b) the input and output traces of the signal are shown. The drawback of this method is that the MIPS doesn't work in the optimal regeneration regime, as the signal power lies outside the optimal range. This is the reason for the reduced output ER of 3.2 dB, while at lower speeds an output ER of 6.2 dB is possible.

Another way to speed up the device, is by reducing the carrier lifetime (τ_c). In Fig. 6(a) the

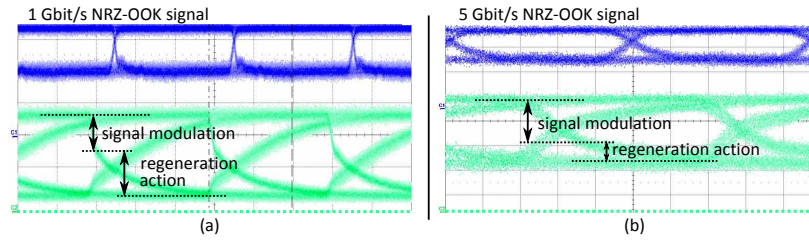


Fig. 5. Eye diagram for regeneration of (a) a 1 Gbit/s signal at 1530nm and a power of -1.5 dBm and of (b) a 5 Gbit/s signal at 1530nm and a power of 6 dBm.

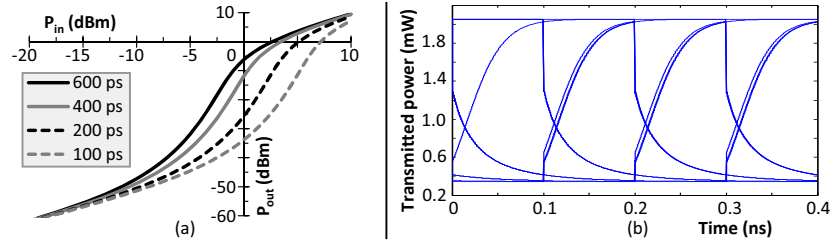


Fig. 6. (a) Simulated transmission curves in the MIPS for different values of τ_c (b) Simulated eye diagram at 10 Gb/s with $\tau_c = 100$ ps.

effect of τ_c on the simulated $P_{out}(P_{in})$ curves is shown. It seems that as τ_c decreases, the required power to bleach the device increases such that the delivered energy during a time τ_c stays the same. In Fig. 6(b) a simulated eye diagram for a signal with an input ER of 2 dB and average input power of 7.2 dBm shows that 10 Gb/s operation is feasible with a reduction of the receiver sensitivity power of 5 dB if the carrier lifetime is brought down from a measured 600 ps to 100 ps. There are several strategies to achieve this. First of all, the width of the III-V membrane waveguide could be brought down. This reduces τ_c due to an increased surface recombination. At the same time the necessary power to bleach the device will go down. Secondly, ions could be implanted to create intermediate energy states in the InGaAs band gap, which can provide for a rapid non-radiative carrier recombination. Finally, by applying a strong electric field across the device, the carriers can be swept out of the QWs, also leading to a reduction of τ_c .

6. Conclusion

In this paper, we have proposed to use the MIPS as an all-optical regenerator. The very high non-linearity in the transmission curve was used to demonstrate passive regeneration of extinction ratio from 2 dB to 6.2 dB, leading to a receiver sensitivity improvement of up to 4.5 dB at a bit rate of 1 Gb/s. Regeneration action was demonstrated across the entire C-band with varying receiver sensitivity improvements since it is dependent on the exact choice of band-edge for the quantum wells. The regenerator was operated with an 8 dB insertion loss (excluding the fiber coupling losses) and required no temperature control. A practical regenerator will be required to operate at 10 Gb/s and give similar regeneration across an entire band of wavelengths (full C-band/L-band) while incurring a minimum insertion loss. Based on the device we tested we believe that lower insertion losses and equal regeneration across the entire C-Band is possible by fine tuning the band gap of the quantum wells. Also, some of the improvement in extinction ratio can be traded for a lower insertion loss. Finally, we have shown, using simulation, that by shortening the carrier lifetime to 100 ps operation at 10 Gb/s is possible. In future work, the proposed strategies to decrease the carrier lifetime will be implemented.